IOP Publishing Journal of Optics

J. Opt. 16 (2014) 125701 (7pp) doi:10.1088/2040-8978/16/12/125701

Multiple primary aberrations effect on donut-shaped laser beam in high NA focusing system

Chen Zhang[1], **Kaige Wang**[1], **Shuang Wang**[1], **Yong Liu**[2], **Wei Zhao**[2], **Xiaoming Chen**[1], **Baole Lu**[1], **Changzhi Gu**[3], **Yong Sun**[4], **Guiren Wang**[2] **and Jintao Bai**[1]

[1] Institute of Photonics & Photon-Technology, Northwest University, Xi'an 710069, People's Republic of China
[2] Mechanical Engineering Department & Biomedical Engineering Program, University of South Carolina, Columbia, SC 29208, USA
[3] Institute of Physics, Chinese Academy of Sciences, Beijing 100080, People's Republic of China
[4] Applied Materials Inc, Santa Clara, CA 95054, USA

E-mail: wanggu@cec.sc.edu, baijt@nwu.edu.cn and wangkg@nwu.edu.cn

Received 30 July 2014, revised 28 August 2014
Accepted for publication 5 September 2014
Published 21 October 2014

Abstract

A donut-shaped laser that is simultaneously impacted by the coma, astigmatism and spherical aberrations in a high NA focusing system is numerically simulated based on the vectorial diffraction theory. The full-width half-maximum, intensity characters, and dimensions of the dark cores of the donut-shaped laser on the focal plane are quantitatively analyzed. The results are highly consistent with the annular-shaped nano-patterns that are experimentally fabricated by our purpose-built laser direct writing system. The mechanism of asymmetric nano-patterns fabricated through laser writing lithography is also revealed.

Keywords: donut-shaped, multiple aberrations, vector diffraction theory, focusing system, nano-pattern
PACS numbers: 42.15Fr, 42.60.Jf, 81.16.Nd

(Some figures may appear in colour only in the online journal)

1. Introduction

In recent years, stimulated emission depletion (STED) microscopic technology has attracted more and more attention from researchers due to its extraordinary discerning capacity in biology and other fields. By combining a donut-shaped laser with a common laser, scientists have improved the resolution to a few nanometers in the far-field optical system [1–4]. The donut-shaped laser beam, which is commonly created by phase plate, is the critical factor for minimizing the point spread function. The shape and size of the dark core of the donut-shaped laser at focus have a direct impact on fluorescence imaging as well as the voxel size of fabricated nanostructures [5, 6].

The influence of primary aberrations on the donut-shaped laser is one of the fundamental problems which deforms the irradiance distribution and might cause a serious decline in resolution. Some scientists have studied the impact of such aberrations, such as the group of R K Singh which analyzed the spherical aberration, coma and astigmatism effects on the focal spot of a Laguerre–Gaussian beam with different topological charges [7–9]. S H Deng studied the aberrations in the simulated emission microscope and revealed the individual primary aberration effects on the donut-shaped depletion laser [10, 11]. The influence of primary aberrations on the 3D polarization of the electric field in the lowest order of the focused radial polarized beam has been studied by D P Biss [12]. And by using the decomposition of the phase of the beam in terms of the Zernike polynomials, J Alda analyzed the characteristic parameters of aberrated laser beams [13]. Nevertheless, these works only concern the separate effects of

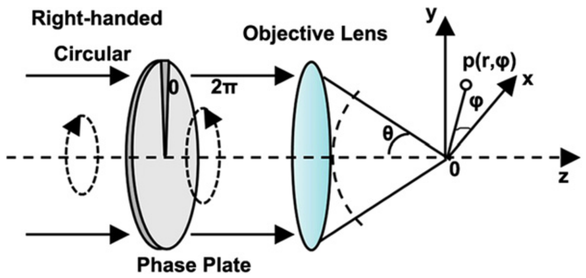

Figure 1. Schematic of focusing Gaussian beam with a phase plate and a high NA objective.

primary aberrations. In fact, the optical system is likely to suffer from multiple influences by primary aberrations at the same time, which might form an entirely different, more complicated depletion beam pattern. In our preliminary simulation study, the light intensity distribution of the donut-shaped depletion pattern on the focal plane was carried out by treating the sum of the coma and astigmatism aberration functions as a multiple aberration function [14].

In this work, the combined influences of coma, astigmatism and spherical aberrations on a donut-shaped Gaussian beam were studied both theoretically and experimentally. The formula of multiple primary aberrations is the product of the exponential functions of coma, astigmatism and spherical aberrations. The depletion laser patterns and their features, including full-width half-maximum (FWHM), intensity and size, were obtained based on the vectorial diffraction theory. The corresponding experimental results were acquired using a purpose-built high NA focusing laser system. Reasonably good matching between the experiments and the calculations not only demonstrates the great utility of theory but also reveals the process mechanism of the donut-shaped laser lithography technology.

2. Theory

Figure 1 shows a schematic model of the generation of a donut-shaped laser beam based on a STED nanoscopic system. The right-handed circular polarized Gaussian beam is chosen and modulated by a vortex phase plate, and the phase changes from 0 to 2π with an anti-clockwise rotation. The laser beam is focused by a high NA (1.4) aplanatism lens.

The electric field vector $\mathbf{E}$ at point p (r_p, φ_p, z_p) near the focus can be expressed by the Debye integral as (1) [15].

$$\mathbf{E}\left(r_p, \varphi_p, z_p\right) = iC \iint_{\Omega} \sin(\theta) \cdot A_1(\gamma, \theta) \cdot A_2(\theta, \varphi) \cdot A_3(\theta, \varphi) \cdot \begin{bmatrix} P_x \\ P_y \\ P_z \end{bmatrix} \cdot \exp\Big[i\Delta\alpha(\theta, \varphi) + z_p \cos\theta + r_p \sin\theta \cos \times \left(\varphi - \varphi_p\right)\Big] d\theta d\varphi \tag{1}$$

where C is a normalized constant; θ is the angle between light direction and optic axis; φ is the azimuthal coordinate at the output plane; and the integral is taken over the exit pupil Ω. $[p_x, p_y, p_z]$ stands for the matrix unit of the polarization of incident light.

$A_1(\gamma, \varphi)$ refers to the amplitude function of the Gaussian light and is given as:

$$A_1(\gamma, \varphi) = I_0 \exp\left(-\gamma^2 \sin^2\theta / \sin^2\theta_{\max}\right) \tag{2}$$

where I_0 is light intensity and assumed to be 1 in the calculation. γ is the truncation parameter that describes the beam inside the physical aperture; it is expressed as $\gamma = a/\omega$ (a is the aperture radius and ω is the beam size at waist). $\gamma > 1$ means the aperture is overfilled, while $\gamma < 1$ means the aperture is underfilled. θ_{max} stands for the maximal semi-aperture angle of the objective, here assigned to 67.07°. $A_2(\theta, \varphi)$ denotes the matrix related to the structure of the imaging lens and equal to $a(\theta)\cdot V(\theta, \varphi)$, where $a(\theta)$ is the apodization factor, equal to $\cos^{1/2}\theta$. $V(\theta, \varphi)$ is the conversion matrix of the polarization from the object field to the image field and expressed as equation (3) [6]:

$$V(\theta, \varphi) = \begin{bmatrix} 1 + (\cos\theta - 1) \times \cos^2\varphi & (\cos\theta - 1) \times \cos\varphi \sin\varphi & -\sin\theta\cos\varphi \\ (\cos\theta - 1) \times \cos\varphi\sin\varphi & 1 + (\cos\theta - 1) \times \sin^2\varphi & -\sin\theta\sin\varphi \\ \sin\theta\cos\varphi & \sin\theta\sin\varphi & \cos\theta \end{bmatrix}. \tag{3}$$

$A_3(\theta, \varphi)$ represents the wavefront aberration function. It is defined as an exponential function acquired by multiplying the separate functions of the coma, astigmatism and spherical aberrations:

$$A_3(\theta, \varphi) = \exp\left[ika_s\left(\frac{\sin\theta}{\sin\theta_{\max}}\right)^4\right] \cdot \exp\left[ika_c\left(\frac{\sin\theta}{\sin\theta_{\max}}\right)^3 \cos\varphi\right] \cdot \exp\left[ika_a\left(\frac{\sin\theta}{\sin\theta_{\max}}\right)^2 \cos^2\varphi\right] \tag{4}$$

where $k = 2\pi n/\lambda$ is the wave number and n is the refractive index of the focal space medium (n = 1.52). The polynomials in (4) refer to the functions of the spherical aberration, coma and astigmatism respectively. We use a_s, a_c and a_a to refer to the aberration coefficients of the spherical aberration, coma and astigmatism, respectively. $\Delta\alpha(\theta, \varphi)$ means the delay of phase. For the vortex phase plate, $\Delta\alpha = \varphi$. In the case of acquiring the intensity on the focal plane, z_p is assigned to 0.

3. Results and discussion

3.1. Simulation

3.1.1. Effect of coma and astigmatism. Since the pattern of the donut-shaped laser beam on the focal plane is strongly influenced by the coma and astigmatism [12], the numerical

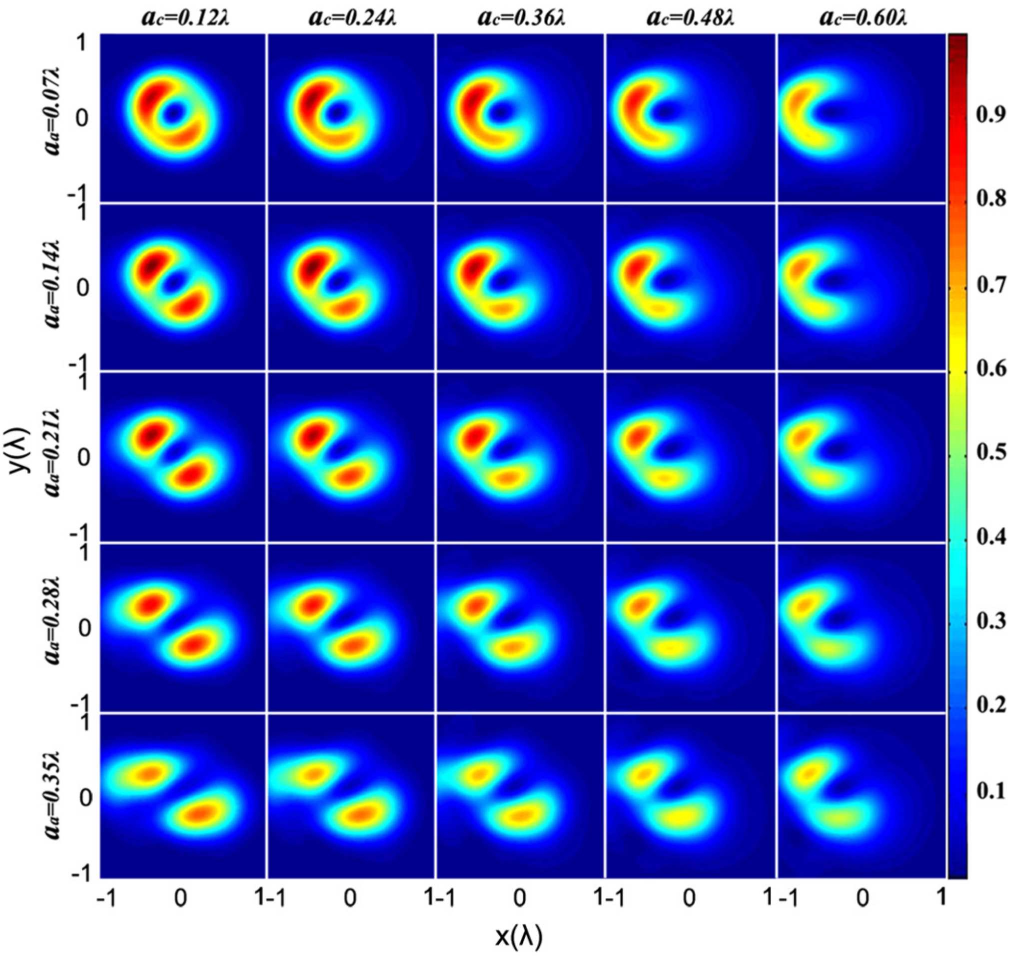

Figure 2. Simulation results of laser patterns on the focal plane with a variety of coma and astigmatism coefficients.

study of the influences of the comatic aberration and astigmatism are prioritized in the study. We use MATLAB for the simulation.

Figure 2 shows the simulated results of the donut-shaped laser on the focal plane with different aberration coefficients a_c and a_a. The selection of the aberration coefficients is based on the aberration tolerance conditions of common focusing systems. The aberration constant a_c of the images, from left to right, increases periodically with a step of 0.12λ, while the a_a of the patterns from top to bottom increases with 0.07λ for each step. The simulated patterns in figure 2 represent the donut-shaped laser influenced by the combined effects of coma and astigmatism, and the parameters a_c change from 0.12λ to 0.6λ and a_a from 0.07λ to 0.35λ.

The beam intensities under all conditions keep symmetrically distributed about the axis x while the donut-shaped laser is influenced only by the comatic aberration. In addition, the dark core moves along the x axis from right to left with increasing a_c (not shown in figure 2). The intensity at the dark region strengthens with increasing a_a when the donut-shaped laser is impacted by the astigmatism alone (not shown in figure 2). With the combined effects of coma and astigmatism, the periphery and the dark core of the donut-shaped laser patterns are transformed to irregular shapes. It can be seen that the laser patterns are neither axial nor central symmetric, and obviously, both the coma and astigmatism aberrations play an important role in the transformation of the patterns. The astigmatism intends to split the pattern into two parts, while the coma contributes to the asymmetric intensity distribution.

Figure 3 illustrates the FWHM variations of the dark core in laser patterns when the constant $a_c \leqslant 0.24\lambda$, $a_a \leqslant 0.14\lambda$. It is obvious that the circles in the patterns are open with $a_c = 0.24\lambda$ and $a_a = 0.14\lambda$; this means that the dark core FWHM isophotes are invalid with $a_c \geqslant 0.24\lambda$ and $a_a \geqslant 0.14\lambda$. When $a_c = a_a = 0\lambda$, the FWHM equals 0.29λ. Since the dark cores change into ellipses, the FWHM should be described with the width in the long axis (W_l) and in the minor axis (W_m). When $a_c = 0.12\lambda$, $a_a = 0\lambda$, $W_l = 0.35\lambda$, $W_m = 0.33\lambda$; $a_c = 0$, $a_a = 0.07\lambda$, $W_l = 0.40\lambda$, $W_m = 0.31\lambda$; $a_c = 0.12\lambda$, $a_a = 0.07\lambda$, $W_l = 0.51\lambda$, $W_m = 0.35\lambda$. Each picture in figure 3 consists of 201*201 pixels. By counting the pixel numbers with MATLAB the area of the dark core can be obtained. The area of the dark core in figure 3(d) is 1.70, 1.37 and 1.28 times larger than that of the dark core in figures 3(a)–(c), respectively. It is apparent that the core under the combined influence of coma and astigmatism is larger than that tolerating separate aberration effects.

Figure 4 reveals the variation of the normalized intensity of laser patterns with different a_c and a_a. Figure 4(a) shows

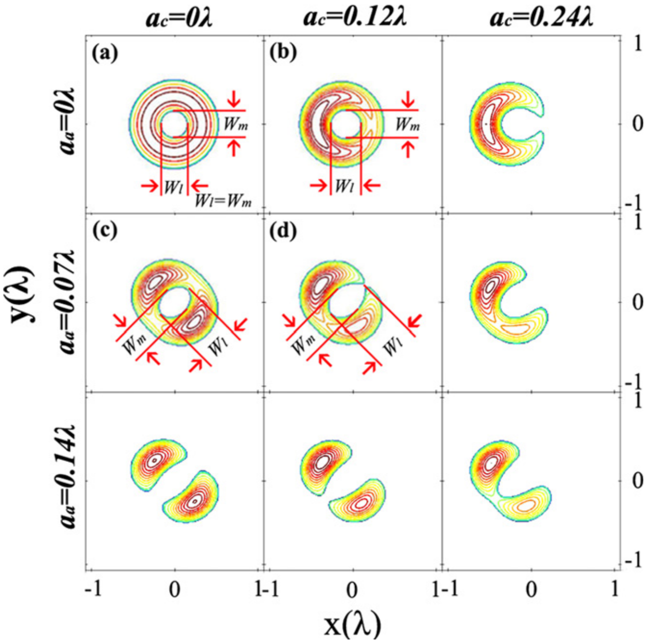

Figure 3. Isophotes for the FWHM of laser patterns calculated with (a) $a_c = a_a = 0\lambda$, (b) $a_c = 0.12\lambda$, $a_a = 0\lambda$, (c) $a_c = 0\lambda$, $a_a = 0.07$, (d) $a_c = 0.12\lambda$, $a_a = 0.07\lambda$.

the change in the maximum intensity in the donut-shaped laser pattern. Figure 4(b) shows the variation of the minimum intensity within the dark cores. The maximum intensities, which have been light enhanced, are converged asymmetrically into a narrow range. Nevertheless, the strengthening of the aberration influence results in the rapid loss of light. The maximum intensity in figure 4(a) is assumed to be 1; it is acquired in the case of $a_c = 0.24\lambda$, $a_a = 0.14$. Figure 4(b) reveals that the minimum intensities of the dark cores increased slightly with the influence of aberrations. The maximum intensity in the dark cores is 0.09 and it is obtained with $a_c = 0\lambda$, $a_a = 0.35$.

3.1.2. Effect of coma, astigmatism and spherical aberration. Generally, a spherical aberration can be induced by poor quality of the immersion oil, the specimen or its mounting medium. The best focus position moves in the axial direction while tolerating spherical aberration effects [15].

Figure 5 shows the intensity distribution on the XZ plane when $a_c = 0.12\lambda$, $a_a = 0.07\lambda$ and a_s changes from 0.16λ to 0.8λ. The coefficient of the spherical aberration is picked on account of the aberration tolerance condition of the focusing system. The amount for each step is 0.16λ. The curve in figure 5 represents the shift of the best focus position with the strengthening effect of the spherical aberration. It can be seen from figure 5 that the best focus position is 0.44λ to 1.81λ departing from $z = 0$ in the axial direction as the a_s increases from 0 to 0.8λ.

Figure 6 presents the laser patterns at the best focal positions of figure 5. The corresponding drawing for the FWHM variation of the dark core is shown in figure 7. It is obvious from figure 6 and figure 7 that the depletion laser pattern, which is experiencing coma and astigmatism influences, is kept in the donut shape. The dimensions of the patterns and the dark core do not change much; meanwhile, the maximum and minimum intensities of the patterns decrease little with the enhancing of a_s.

Figure 8 reveals the change of the dark core area and intensity of the donut-shaped pattern. Figure 8(a) shows that with the combined effect of the primary aberration the dark core area is 1.66 to 1.75 times bigger than that of the ideal donut-shaped pattern, while it is 0.98 to 1.03 times larger than the pattern of $a_s = 0$. With the increasing a_s the dark core shrinks slightly. Figure 8(b) illustrates that the maximum normalized intensity of the donut-shaped pattern $I_{\max}$ has been reduced from 0.98 to 0.85 when the spherical aberration increases. Meanwhile, the minimum intensity of the dark core of the depletion beam remains 0.

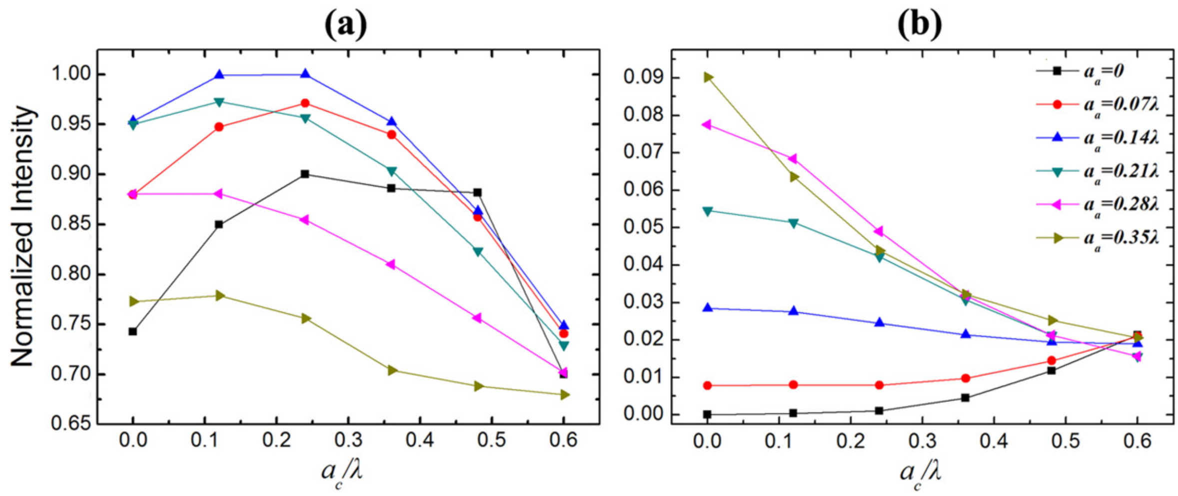

Figure 4. Variations of normalized intensity under different situations. (a) Maximum intensity within the donut-shaped laser beam. (b) Minimum intensity within the dark core.

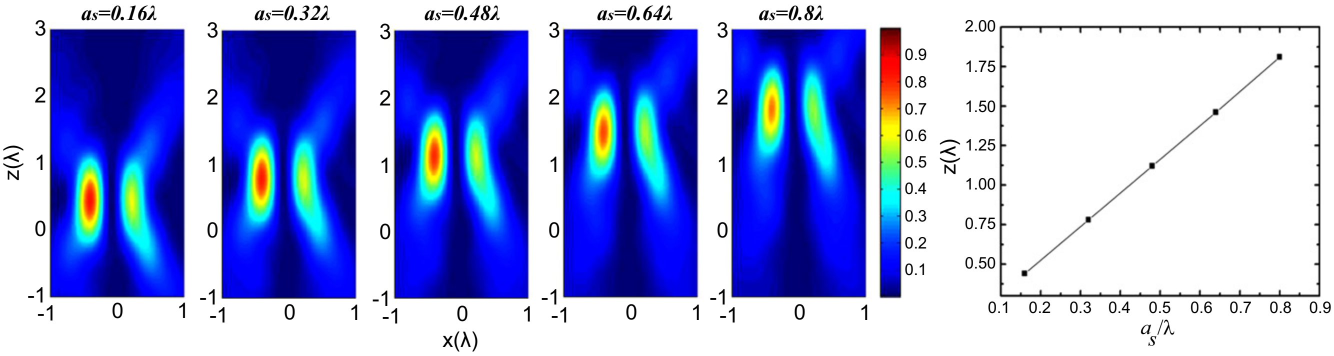

Figure 5. Axial intensity distribution of donut-shaped pattern tolerating multiple primary aberrations.

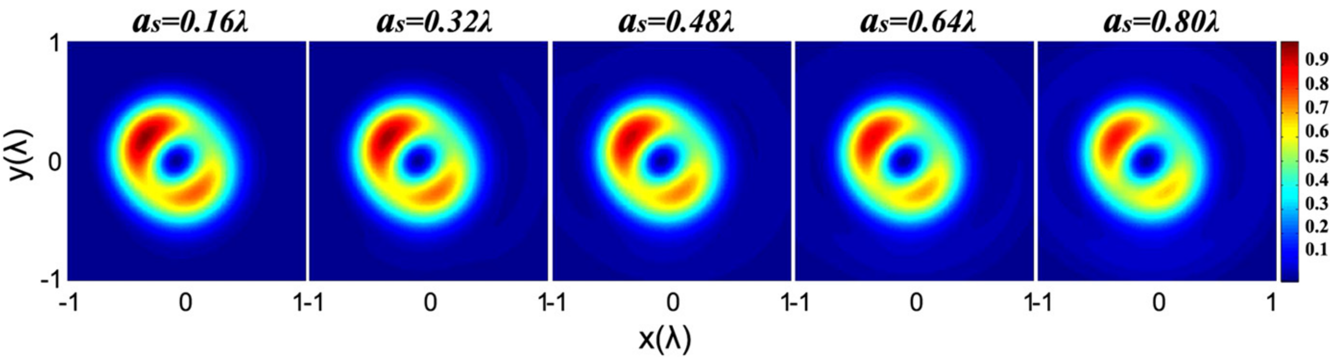

Figure 6. Intensity distribution for multiple aberration impacted laser patterns at the best focus position.

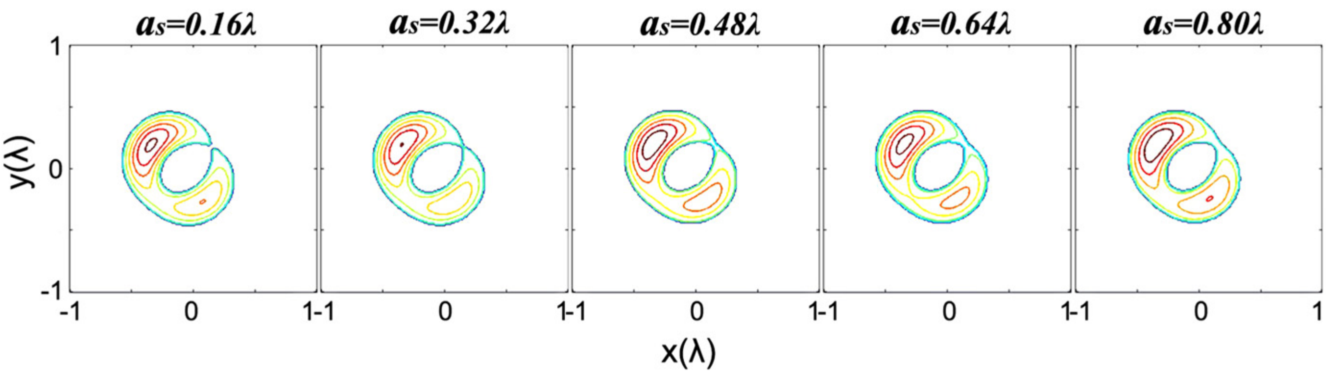

Figure 7. Isophotes for the FWHM variation of laser patterns impacted by multiple aberrations.

3.2. Experiment

Based on a purpose-built CW laser-based far-field nanoscopic system with a high NA objective we have achieved a kind of nanostructure array, i.e. nanopillars. The fabricated nanostructure can offer reasonable and convincing proof of the simulation results. In the experiment, a laser with 532 nm wavelength (16 μw at objective pupil) was employed to expose on a positive tone photoresist coating (OIR906, Fujifilm Electronic Materials USA, Inc.). A vortex phase plate with phase changes from 0 to 2π in the anti-clockwise direction was inserted into the light path (identical to the theoretical model). The laser was right-polarized at the pupil of the objective (Apoplan 100×/1.4, Olympus Optical Co., Ltd, Japan).

Figure 9 shows a comparison of the simulated intensity distributions and the experimentally fabricated nano-patterns imaged with atomic force microscopy (AFM). Considering that the spherical aberration is primarily induced by the immersion oil or the specimen, the a_s is assumed to be 0.04λ in the calculation. By using MATLAB the best focus position can be obtained, $z \sim 0.15\lambda$. Figure 9(a) is the calculated pattern with $a_s = 0.04\lambda$, $a_c = 0.1\lambda$, $a_a = 0.05\lambda$ and $z = 0.15\lambda$. It is seen that the intensity is asymmetrically distributed in this condition. The upper-left part of laser pattern possesses a higher light intensity and distribution region. The light intensity in the lower-right part of the pattern is lower, and the area that the light covers is smaller as well. In addition, there is an area with weak light between the two bright areas as pointed out in figure 9(a). Figure 9(b) shows the AFM

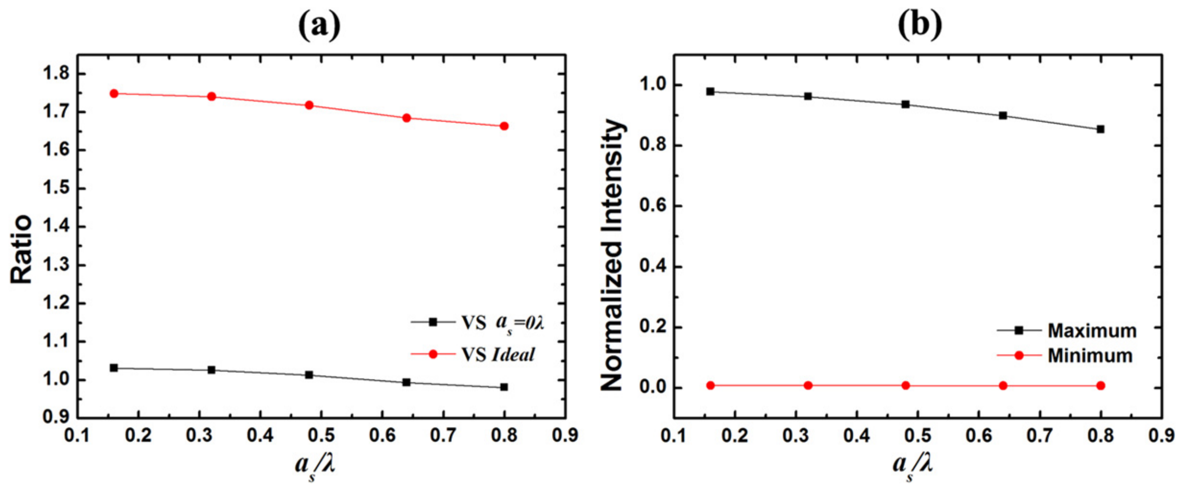

Figure 8. Variation of the donut-shaped pattern with increasing a_s. (a) The area of dark core. (b) The intensity of pattern.

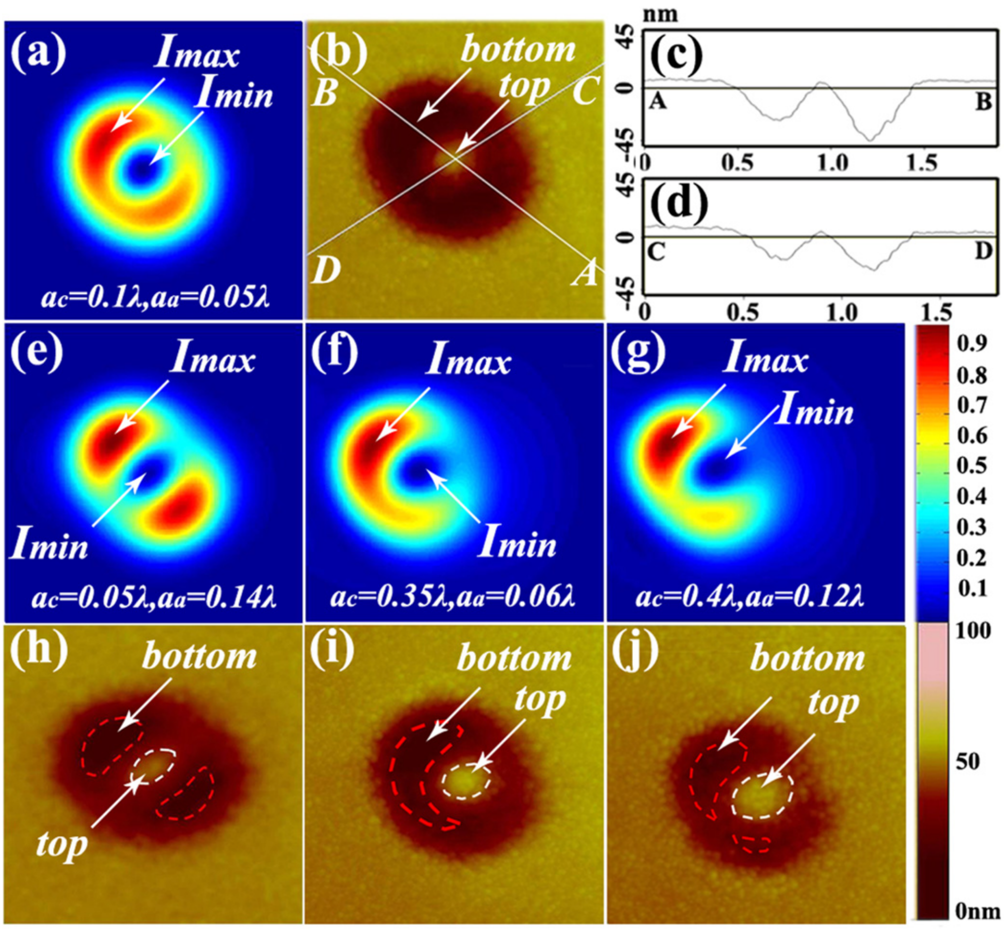

Figure 9. Comparison between the results of simulation and experimental fabrication. (a) Simulation with $a_s = 0.04\lambda$, $a_c = 0.1\lambda$, $a_a = 0.05\lambda$, $z = 0.15\lambda$. (b) The AFM images for the corresponding fabrication pattern of (a). (c), (d) Cross-sections along lines AB and CD respectively. Simulated donut-shaped pattern with $z = 0.15\lambda$ and (e) $a_s = 0.04\lambda$, $a_c = 0.05\lambda$, $a_a = 0.14\lambda$; (f) $a_s = 0.04\lambda$, $a_c = 0.35\lambda$, $a_a = 0.06\lambda$; (g) $a_s = 0.04\lambda$, $a_c = 0.4\lambda$, $a_a = 0.12\lambda$. (h), (i), (j) AFM scanning images of experimentally fabricated nano-patterns assumed to correspond to (e), (f) and (g) in sequence.

scanning image of a fabricated nano-pattern. It can be seen that there are many similarities between figures 9(a) and (b). First, the periphery of the nano-pattern has the same pattern as the simulated laser pattern. Second, the characters of the depth in nano-pattern are identical to the intensity distributing features in the simulation. Just as illustrated in figure 9(b), the line AB passes through the bottom and the top of the nano-pattern, while the line CD goes across the top and the shallow parts of the nano-pattern. The corresponding cross-section profiles of the surface along AB and CD are revealed in figures 9(c) and (d) respectively. It is obvious that the upper-left part of the nano-pattern is deeper and larger than the rest, which indicates a larger area with higher light intensity. The shallow structure in the upper-right part of the nano-pattern corresponds to the weak part in figure 9(a). It should be noted that because of the conical shape of the AFM probe tip, the height of the nano-pattern is only relatively revealed. Let $z = 0.15\lambda$. Figure 9(e) is the calculated result with $a_s = 0.04\lambda$, $a_c = 0.05\lambda$ and $a_a = 0.14\lambda$. Figure 9(f) is the result obtained with $a_s = 0.04\lambda$, $a_c = 0.35\lambda$ and $a_a = 0.06\lambda$. Figure 9(g) is the simulated result carried out with $a_s = 0.04\lambda$, $a_c = 0.4\lambda$, and $a_a = 0.12\lambda$. Apparently, the focal laser spots with these parameters possess significant similarities to the nano-patterns in figures 9(h)–(j) sequentially; nano-patterns are very likely to be fabricated by the donut-shaped laser patterns tolerating wavefront aberrations such as figures 9(3), (f) and (g). It should be noted that there are some differences between the practical aberration coefficients and the simulation conditions due to the experimental conditions being much more complex.

4. Conclusion

The combined influence of coma, astigmatism and spherical aberrations on the donut-shaped laser beam in the focus plane for an optical super-resolution, far-field nanoscopic system has been studied by numerical simulation based on the vectorial diffraction theory. The physical parameters of the laser at focus, such as the FWHM, dimensions and intensity of the dark core, are analyzed quantitatively in detail. It is found that the variation of the donut-shaped laser is complicated. The features are seriously determined by the factors at play, i.e. a_c, a_a and a_s together. The simulation results are compared with the corresponding nanopillar structures fabricated using a purpose-built far-field nanoscopic system. The high consistency between the experiments and the simulations partly reveals the process mechanism of the direct writing technology using the donut-shaped laser beam. The study could provide an insight into far-field optical super-resolution technology.

Acknowledgments

This work was supported by the Major Research Plan of the Natural Science Foundation of China (Granted No. 91123030, No. 61378083), the International Science & Technology Cooperation Program of China (granted No. 2011DFA12220), and NSF's MRI CBET-1040227, USA.

References

[1] Hell S W 2007 *Science* **316** 1153
[2] Reuss M, Engelhardt J and Hell S W 2010 *Opt. Express* **18** 1049
[3] Scott T F, Kowalski B A, Sullivan A C, Bowman C N and McLeod R R 2009 *Science* **324** 913
[4] Cao Y Y, Gan Z S, Jia B H, Evans R A and Gu M 2011 *Opt. Express* **19** 19486
[5] Hao X, Kuang C F, Wang T T and Liu X 2010 *J. Opt.* **12** 1
[6] Zhang C, Wang K G, Bai J T, Wang S, Zhao W, Yang F, Gu C Z and Wang G R 2013 *Nanoscale Res. Lett.* **8** 1
[7] Singh R K, Senthilkumaran P and Singh K 2008 *Opt. Commun.* **281** 5939
[8] Singh R K, Senthilkumaran P and Singh K 2008 *J. Opt. A: Pure Appl. Opt.* **10** 1
[9] Singh R K, Senthilkumaran P and Singh K 2009 *Opt. Laser. Eng.* **47** 831
[10] Deng S H, Liu L, Cheng Y, Li R X and Xu Z Z 2010 *Opt. Express* **18** 1657
[11] Deng S H, Liu L, Chen Y, Li R X and Xu Z Z 2009 *Opt. Express* **17** 1714
[12] Biss D P and Brown T G 2004 *Opt. Express* **12** 384
[13] Alda J, Alonso J and Bernabeu E 1997 *J. Opt. Soc. Am.* A **14** 2737
[14] Zhang C, Wang K G, Bai J T, Liu Y and Wang G R 2013 *Opt. Photon. J.* **3** 1
[15] Born M and Wolf E 2003 *Principles of Optics* (Cambridge: Cambridge University Press)